Scientific Research Publishing

American Journal of Analytical Chemistry, 2023, 14, 326-349
https://www.scirp.org/journal/ajac
ISSN Online: 2156-8278
ISSN Print: 2156-8251

Microwave-Assisted Transition Metal Nanostructure Synthesis: Power-Law Signature Verification

Victor J. Law*, Denis P. Dowling

School of Mechanical and Materials Engineering, University College Dublin, Dublin, Ireland
Email: *viclaw66@gmail.com

How to cite this paper: Law, V.J. and Dowling, D.P. (2023) Microwave-Assisted Transition Metal Nanostructure Synthesis: Power-Law Signature Verification. *American Journal of Analytical Chemistry*, **14**, 326-349.
https://doi.org/10.4236/ajac.2023.148018

Received: July 16, 2023
Accepted: August 27, 2023
Published: August 30, 2023

Abstract

A power-law ($y = cx^n$) signature between process energy budget (kJ) and process energy density (kJ·ml^{-1}) of microwave-assisted synthesis of silver and gold nanostructures has been recently described [Law and Denis. AJAC, 14(4), 149-174, (2023)]. This study explores this relation further for palladium, platinum, and zinc oxide nanostructures. Parametric cluster analysis and statistical analysis is used to test the power-law signature of over four orders of magnitude as a function of six microwave applicator-types metal precursor, non-Green Chemistry synthesis and claimed Green Chemistry. It is found that for the claimed Green Chemistry, process energy budget ranges from 0.291 to 900 kJ, with a residual error ranging between −33 to +25.9 kJ·ml^{-1}. The non-Green Chemistry synthesis has a higher process energy budget range from 3.2 kJ to 3.3 MJ, with a residual error of −33.3 to +245.3 kJ·ml^{-1}. It is also found that the energy profile over time produced by software controlled digestion applicators is poorly reported which leads to residual error problematic outliers that produce possible phase-transition in the power-law signature. The original Au and Ag database and new Pd, Pt and ZnO database (with and without problematic outliers) yield a global microwave-assisted synthesis power-law signature constants of $c = 0.7172 \pm 0.3214$ kJ·ml^{-1} at x-axes = 0.001 kJ, and the exponent, $n = 0.791 \pm 0.055$. The information in this study is aimed to understand variations in historical microwave-assisted synthesis processes, and develop new scale-out synthesis through process intensification.

Keywords

Microwave-Assisted Synthesis, Pd, Ag, Pt, Au, ZnO, Power-Law, Residual Error, Statistical Analysis, Parametric Cluster Analysis

1. Introduction

Since the 1970s microwave rapid synthesis of organic materials (Gedye *et al.* (1988) [1], Gedye *et al.* (1991) [2]) and inorganic materials (Rinaldi *et al.* (2015) [3]) has become a well-established chemical synthesis route. The emergence of Green Chemistry with its twelve principles has embedded itself within this microwave synthesis approach (Grewal *et al.* (2013) [4]. In the case of metal precursor and reactants within a colloid form transition-metal nanostructure products, the synthesis process feeds into the linear economy model of nanoscience and nanotechnology (*i.e.*, energy, food, sensor, medicine, and medical-diagnostics (Priecel and Lopez-Sanchezl (2018) [5]. It is generally thought that the microwave-assisted reaction pathways within the colloid involve both dielectric volume heating and ionic conduction within the precursors and reactants and possible resistive heating of the metal atoms themselves within the nucleation, growth, and subsequent capping stages. An understanding of these selective heating pathways in terms of the sixth principle of Green Chemistry (reduction in energy usage and an increase in energy efficiency that are recognized for environmental and economic impact) and its implementation through process intensification (minimization of reactor size, conversion from batch to continuous flow and the utilization of microwave technology) is of growing interest and importance.

In 2022 it was shown that for microwave-assisted processes operating at a running frequency f_o = 2.45 ± 0.05 GHz (~12.2 cm), energy phase-space projection that maps the process energy budget (kJ) and energy density (kJ·m^{-1}) can be used to define the sixth principle (Law and Dowling (2022) [6]). In the following year (2023), the energy mapping technique was applied to historical "non-thermal" microwave-assisted microorganism inactivation experiments and their reconstruction using pseudo microorganism suspension, in this case, the eco-friendly and benign solvent "water" (H_2O) (Law and Dowling (2023) [7]). More recently it has been shown that using log-log coordinates, historical microwave-assisted synthesis of gold (Au), and silver (Ag) nanostructure data (n = 30) may be visualized (Law and Dowling (2023) [8]) with the addition of fitting in a general power-law function (Equation (1)) where small and large events are common over four orders of magnitude in both x- and y-axes.

$$y = cx^n \tag{1}$$

where y is the parameter of interest, c and n are the coefficient and the exponent of the equation. In this case, without recourse binning or Pareto cumulative distribution function (Hanel *et al.* (2017) [9]), a fit of $y = 0.3293x^{0.846}$ is obtained. The goodness of fit obtained through linear regression (R^2) = 0.7923, however it is not used as an indicator of accuracy **Figure 1**.

In 1936, J.S. Huxley and G. Teissier [10] first coined the word Allometry for the measuring relative growth in biological systems, since then allometric scaling has expanding in to the scientific of physiology and bibilometic studies (W.A. Calder. III (1981) [11], Stumpf and Porter (2012) [12], Dong *et al.* (2017) [13]).

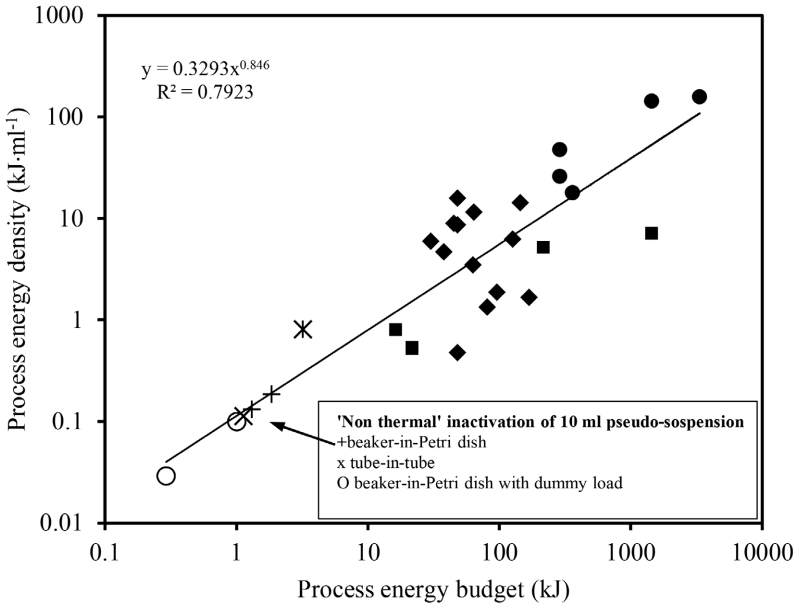

Figure 1. Log-log energy phase-space projection of Au and Ag claimed Green Chemistry and non Green Chemistry for the axial field helical antenna system (star), TCMC systems (black square), turntable loaded digestion systems (black circle), and microwave oven (black diamond), and "non thermal" inactivation of microorganisms within microwave ovens (plus sign, star and open circles [8]).

In all cases the exponent defines the type of scaling relationship between *y* and *x*; < 1 means the energy transfer increases slower (negative, or, *hypoallomerty*) than the applied process energy increase; an exponent = 1 would mean that relationship is *isometry*; and if the exponent > 1 then the energy transfer increase faster (positive, or *hyperallometry*) than the applied process energy increase. Thus, the mathematical response model ($y = 0.3293x^{0.846}$, $R^2 = 1$) implies that the energy transferred to the suspension volume is subcritically proportional to the process energy budget and is Scale Free throughout the process energy budget range therefore preserving some underlying invariant microwave-assisted synthesis.

From a statistics and probability perspective the power-law signature is a 0-dimensional (0-D) representation of the underlying microwave synthesis processes. However, the power-law signature encompasses different microwave applicators-types used (domestic microwave oven, temperature controlled microwave chemistry (TCMC) applicator, digestion applicator, and the axial field helical antenna applicator (Discover2), metal precursors, and synthesis chemistries [8]. Therefore it is reasonable to postulate that the power-law signature may contain phase-transitions (PT) arising from the applicator-type and the mode that it is used (batch, or, continuous flow) or the way the microwave power is applied. For example, commercial Digestion applicators use proprietary software to vary the pulse width modulation (PWM) of the cavity-magnetron voltage. In practices this requires the cavity-magnetron instantaneous or continuous wave (CW, 100% duty cycle) to be applied in the temperature ramp-up period, and < 100% duty cycle in the temperature hold period. The lack of re-

porting of ramp-up period and in the hold period power [14] [15] [16] [17] [18] has lead to the use of an estimated 75% of the cavity-magnetron CW rated power when calculating the process energy budget (power multiplied by process time) [8].

The uncertainty in the actual value of process energy budget raises a number of questions. First, are PTs present, and second are outliers' presents in original database. Both PT and outliers are problematic as they may be natural deviations in the database, or due to poor recording and reporting of experimental conditions.

Given these questions, the aim of this work is threefold. First to identify and classify PTs within the original microwave-assisted synthesis database (n = 30) [8]. This database is now referred to as **Database A**. Second to apply the same tests to a larger database (n = 50) to establish if PTs are an artifact of sample size. This new database is referred to as **Database B** (n = 30 + 20 = 50), where the additional data pertains to microwave-assisted synthesis of palladium (Pd) and platinum (Pt), and zinc oxide (ZnO) nanostructures, plus an additional microwave applicator (ERTEC, Wrocław, Poland). The transition-metals Pd and Pt are chosen as they are in the same Group (V and VI) and electron orbital filling (10 and 11) as Ag and Au, hence they would be expected to have similar energy phase-space properties. To extend this hypothesis, Zn is chosen as it is a close neighbor (Group IV with 12 electrons in its d-orbital). Zinc oxide is also chosen as it is of great interest due to its *n*-type wide band gap (~3.37 eV at room temperature) semiconductor property [19]. **Figure 2** shows the relative *d*-block position and atomic number for these five transition metals within the modern Periodic Table. Third, two application are compared directly for real comparison purposes. The applicator is the Samsung microwave oven (CE2877) that is used for the synthesis of Pt [20] and Ag nanostructures [21], and the Discover2 applicator used in both batch and continuous and mode.

The building of **Database B** (n = 50) follows the same procedure as **Database A** (n = 30) as set out in [8]: that is the data extracted from each new published paper is represented by a new data entry into an Excel spread sheet. The data includes: first author and year of publication, applicator-type, metal precursor, Claimed Green Chemistry, Non-Green Chemistry, calculated process energy budget, and process energy density. To calculate the process energy budget and

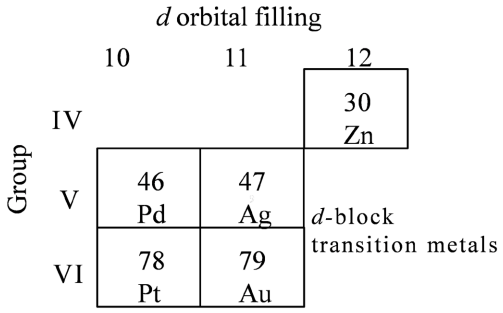

Figure 2. *d*-block transition metals (Zn, Pd, Ag, Pt, and Au) relative position within the modern periodic table. Atomic number, Group, and *d*-orbital electron filling are given.

process energy density, each paper must provide information on the estimation of microwave power, microwave irradiation time, and reactant quantities. A total of thirty new publications pertaining to microwave-assisted synthesis of Pd, Pt, and ZnO nanostructures were investigated, of which only twenty fitted the criteria. The ten papers not used [22]-[31] were published between 2004 and 2023 thus indicting that full power conditions are still not being reported. Secondary data, temperature, and working pressure were recorded. Where the primary and second data was ambiguous in the publication text, private communication with the publication authors were sought and is given in the text. In addition, on-line microwave applicator manufactures manuals are used to refine the information within the accepted twenty publications.

The remainder of this work is constructed as follows. Section 2 details the analysis methodology used. The test results for **Database A** are given in Section 3. The building of **Dataset B** and test results is given in Section 4. Section 5 provides an estimation of the global (average of **Database, A, B and $B_{adjusted}$**) microwave-assisted synthesis power law. Section 6 is a summary and outlook of this work. To add the reader, only one of the applicators is operated in the continuous flow (Discover2) mode is heighted in the text, the remaining applicators are operated in the batch mode. In addition, full details of **Database A** may be found in [8].

2. Analysis Methodology

It is generally regarded that classical linear regression analysis is based on the assumption that the dataset under investigation has a normal distribution (bell-shaped) where the sum of data points either side of the arithmetic mean is equal zero ($\Sigma = 0$). In the real-world, however, outliers distort the normal distribution, resulting in the summation of all data points either side of the arithmetic mean not equal to zero ($\Sigma \neq 0$) in most cases. Moreover where a dataset exhibits a power-law signature the distribution is non-linear (for example a Pareto distribution that contains a long and flat tail), meaning that summation of the data points will never equate to zero. Indeed it is well documented that outliers distort both group variance and group arithmetic mean [9] [10] [11], and Andriani and McKelvey (2009) [32], particularly when attempting to verify a power-law over a limited magnitude range (< 2 to 2.5; in both x and y axes) due to either limited sample size, or the complex nature of physiological, chemical, and geophysics datasets. For example in the plasma etching of semiconductors it s known that competing reactive ion etching and decomposition processes limit the power-law magnitude range < 2 [33] [34]. Whereas in the field of high density pulse laser ablation, where energy transfer processes dominate, rather than physiological and chemical processes, it is found that the propulsion velocity of tin microdroplets has a power-law dependency over 3 orders of magnitude with laser power [35]. Simulations performed with the RALEF-2D radiation-hydrodynamic code indicate the magnitude is possibly limited by the applied laser pulse width (10

nanoseconds). Lastly, bibilometric studies within the scientific fields of physics, mathematics and econometric have produced a scale range of 8 to 10 orders of magnitude [13]. Hence a linear regression analysis approach to experimental datasets exhibiting a power-law signature is nontrivial as complex processes within the dataset has the potential to influence variance, and produce an unstable arithmetic mean.

Acknowledging this complexity, this study attempts to identify and verify deterministic features within the power-law signature of **Database A** and the enlarged sample size of **Database B**. To this end Microsoft Excel spread sheet software is used to collate and display the datasets within a XY scatter plot, flowered by fitting a linear regression power function trend-line to the data. The trend-line is then modeled using the Excel power function (=POWER (A1, 2, 3, Y1) * Z2), where A1, 2, and 3 are the cell coordinates, and the cells Y1 and Z2 are the values of the c and n constants of Equation (1). This power function, straighten-out the power function into a horizontal 0-D model identity-line that represents the process energy density prediction at each process energy budget value (Figure 3).

Two evaluation tests are used to detect PT and outliers from the characteristics of normal objects within each database. The tests are as follows:

1) 1-dimesitional (1-D) test is made on the disagreement, or difference, between the observed process energy density values and the 0-D model data points. The tests are performed on **Database A**, and **B** in high-dimensional space of a residual plot, where the vertical axes represent the observed difference and the horizontal axes represents the 0-D model identity-line. The disagreement (± from the identity line) is quantified using the ± 3 Sigma rule of thumb (68%, 95%, and 99.7%) where data points close to, or beyond, the ± 3 Sigma limit are

=POWER(D3,I3)*I4

	A	B	C	D	E	F	G	H	I	J	K	L	M	N	O	P	Q
1	**X-Y scatter graph**			**X-Y Graph**													
2	**Paper**	**Appliactor**	**Load**	**Energy (x-**	**Energy density**	**Model**	**Difference (G - E)**	**Change sign**	**Power constant**								
3	Law2023	MO	dummy load	291	29.1	59.8	30.7	-30.7	**0.764**								
4	Law2023	MO	dummy load	1000	100	153.5	53.5	-53.5	**0.7837**								
5	Law2023	MO	tube-in tube	1129	112.9	168.4	55.5	-55.5									
6	Law2023	MO	beaker	1310	131	188.7	57.7	-57.7									
7	Law2023	MO	beaker	1856	185.6	246.2	60.6	-60.6									
8	Bayazit2016	Discover	Au-rods	3200	810	373.3	-436.7	436.7									
9	Rademacher2022	Discover	Pd-shard	120000	600	5951.7	5351.7	-5351.7									
10	Liu2019	MO	Zn-flower	120000	2400	5951.7	3551.7	-3551.7									
11	Cao2004	MO	Zn-flower	126000	31500	6177.8	-25322.2	25322.2									
12	Li2011	MO	Zn-flower	180000	3150	8112.9	4962.9	-4962.9									
13	Cai2023	MO	Zn-flower	204000	887	8927.0	8040.0	-8040.0									
14	Cao2011	MO	Zn-flower	204000	2040	8927.0	6887.0	-6887.0									
15	Hasanpoor2015	MO	Zn-flower	380000	3800	14358.3	10558.3	-10558.3									
16	Aljaafari2020	MO	Zn-flower	216000	2160	9325.5	7165.5	-7165.5									
17	Elazab2018	MO	PdCuO	7500	348.8	715.6	366.8	-366.8									
18	Nadagouda2007	MO	Au	16200	6000	1288.9	-4711.1	4711.1									
19	Yazmin2014	MO	Au	21600	4725	1605.7	-3119.3	3119.3									
20	Nadagouda2017	MO	Au-PCH	21600	9000	1605.7	-7394.3	7394.3									
21	Bhosle2015	MO	Au-flower	30000	8727	2063.8	-6663.5	6663.5									
22	Shah2019	MO	Au-hex	37800	16000	2462.4	-13537.6	13537.6									
23	Jyohai2020	MO	Ag	45000	480	2813.2	2333.2	-2333.2									
24	Nago2015	MO	Au-tri	64000	3500	3681.9	181.9	-181.9									
25	Bhosle2015	MO	Au	64000	11636	3681.9	-7954.5	7954.5									

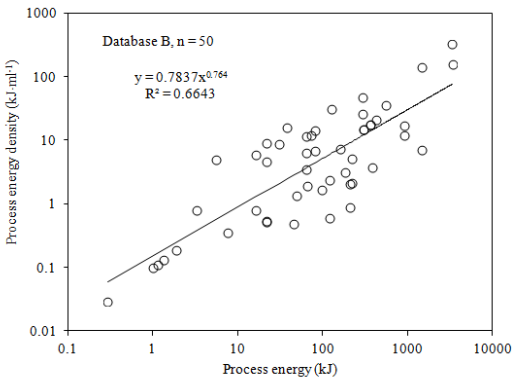

Figure 3. A section of the Excel spread-sheet showing a section of Database B collated microwave-assisted synthesis data for energy phase-space projection. The code at the top of figure (ringed in red) depicts the Excel =Power model. In this example the Difference (G minus E) columns require * −1 to obtain the correct sign.

classed as problematic outliers and require further examination as outliers strongly depends on a detailed understanding of their experimental origins, see Sections 3, 4, and 5.

2) 2-demesional (2-D) non-parametric cluster analysis as described by Tynan *et al.* (2009) [36], and Law *et al.* (2010) [37] is used to quantify group residual errors. The basic assumption used here is that outliers are few in number and their x, y coordinate distance from a cluster is some multiples of the normal distance between data points (as measured by the metric) within a cluster. However, in the LabVIEW Vision builder software was used to threshold the Microsoft Excel data points into cluster and separate out outliers using their *x, y* pixel connectivity on a graph 2-D plane. This was then followed by computing the information-based entropy of the cluster. In this work, the 2-D parametric cluster analysis using three metrics is performed on the Microsoft Excel data points presented in a high-dimensional of the residual plot, but this time the data points are pre-assigned into N groups (applicator-type, water-MO, NS-metal precursor, claimed Green Chemistry, and non-Green Chemistry).

The information gain from these tests along with detailed knowledge of the PT and outliers origins is used to decide if the PT and outliers are part of the data natural variation, or are due to errors in the reporting of experiment data. In the latter case this problematic outliers are cleaned (filtered) to produce an adjusted **Database B** ($\mathbf{B}_{\mathbf{adjusted}}$). The power-law signatures of **Database A** and **B** and $\mathbf{B}_{\mathbf{adjusted}}$ are compared and global a microwave-assisted synthesis power-law is calculated.

3. Database A (n = 30)

Figure 4 shows the residual plot for **Database A**. In this plot the data points are colored coded into five applicator-types (water-MO, NS-Discover2, NS-MO, NS-TCMC, and NS-digestion, MO refers to microwave oven and NS refers to nanostructures). Visually it is observed that the data points have a non-null, distribution around the model identity-line. For the water-MO (five open circles) and the NS-Discover2 that is operating in the continuous mode (one yellow circle) all exhibit a similar disagreement value from the model identity-line. Whereas, the NS-MO (thirteen green diamonds) and the NS-TCMC (five blue triangles) form clusters around the model identity-line, with the TCMC-102 applicator [38] having the greatest negative disagreement (1440 kJ, -46.2 $kJ{\cdot}ml^{-1}$). It is worth noting that the remaining four tightly grouped applicators are Shikoku Keisoku SMW-064 applicators synthesizing Ag nanostructures. Lastly the Digestion applicators (six red squares) generate an open cluster with the MARS-6 applicator synthesizing Au nanostructures [18] having the greatest disagreement (+90.5 $kJ{\cdot}ml^{-1}$) with the model identity-line. The MARS-5 applicator [14] forms the second greatest disagreement (+50 a $kJ{\cdot}ml^{-1}$). The remaining four applicators (Aton Paar Multiwave, Aton Parr Pro, and two μSnth form an open cluster in the range of 280 to 360 kJ, +1 to +34 kJ $kJ{\cdot}ml^{-1}$.

Figure 5 shows a residual plot of **Database A**, but this time color coded in to three groups (water-MO (five open circles), NS-Au (fourteen yellow circles) and NS-Ag (blue circles). The notation MO, and NS have the same meaning as in Figure 4. Visually it is observed that the thermal microwave-assisted processing of water-MO group has the same disagreement values close to the model identity-line. The NS-Au and NS-Ag synthesis groups are spread either side of the model identity-line with two of NS-Ag cluster having the greatest positive disagreement (+90.59 kJ·ml^{-1}) for the MARS-6 applicator, and the TCMC-102 applicator having greatest negative disagreement (−46.2 kJ·ml^{-1}).

Figure 6 shows a residual plot for **Database A**, the data is divided into the

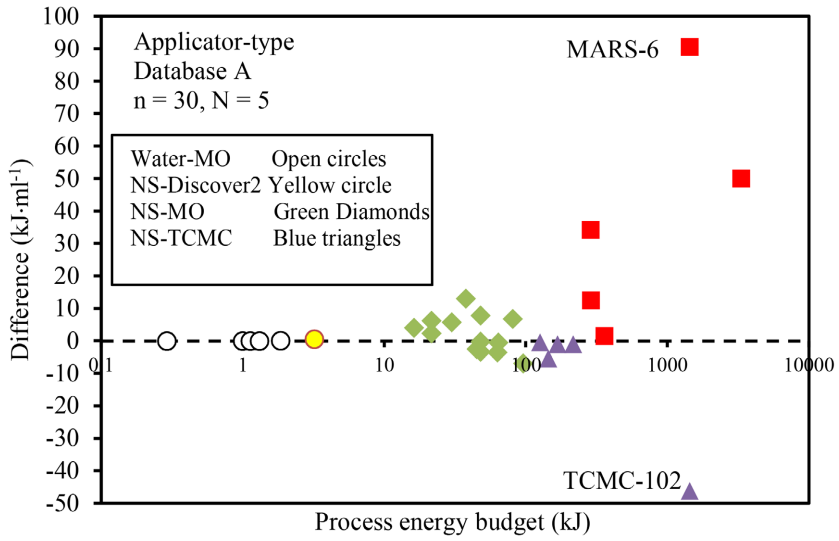

Figure 4. **Database A**; residual error analysis for five applicator-type (water-MO, NS-Discover2, NS-MO, NS-TCMT, and NS-Digestion; MO refers to microwave oven and NS refers to nanostructures.

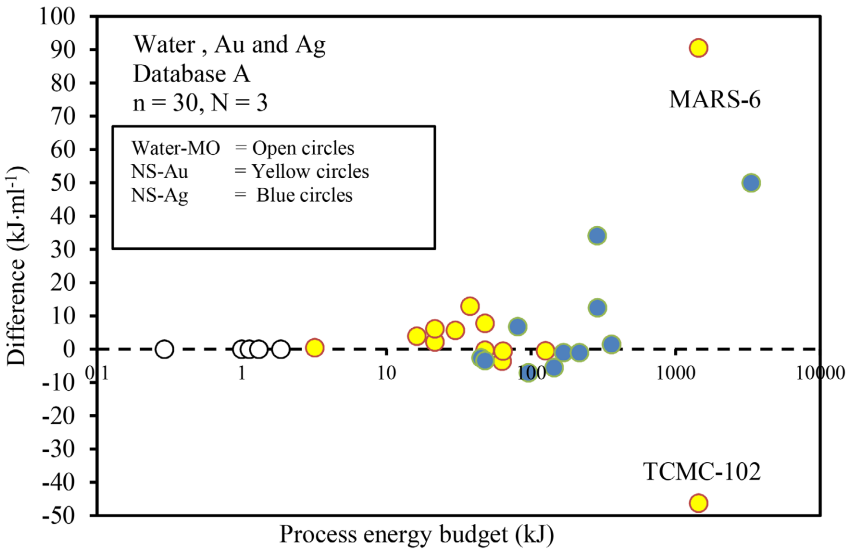

Figure 5. **Database A**; residual error analysis for water-MO (open circles), NS-Au precursor (yellow circles) and NS-Ag precursor (blue circles).

following: claimed Green Chemistry (green circles) and non-Green Chemistry (red squares). Water is considered as a universal polar solvent that is nontoxic and environmentally benign is included in the Green Chemistry group. Visually it is observed that the non-Green Chemistry data is spread along the model in-dentify-line up to approximately 200 kJ process energy budget, from where the disagreement diverges strongly to −46.2 kJ·ml^{-1} kJ for the TCMC-102, and up to +90.5 kJ·ml^{-1} for the MARS-6 applicator.

A visual comparison of the residual error data points in Figures 4-6 suggests two possible PTs. The first (PT_1) is between the water-MO plus Discover2 (continuous flow) groups and NS-MO applicator-type group. The second PT_2 is located between the NS-TCMC and NS-Digestion group boundaries.

From a Sigma test point of view, Table 1, reveals twenty six of the data points fall within ± sigma, three within the ± 2 to ± 3 Sigma limit and one at the ± 3 Sigma limit indicating that the power-law residual error has a uniform distribution with the problematic MARS-6 applicator outlier at the ± 3 Sigma limit. Further consideration of PT_1 and PT_2, and the problematic outlier is given in Section 4.

4. Database B (n = 50)

For completeness this section provides a description of the reactants, microwave

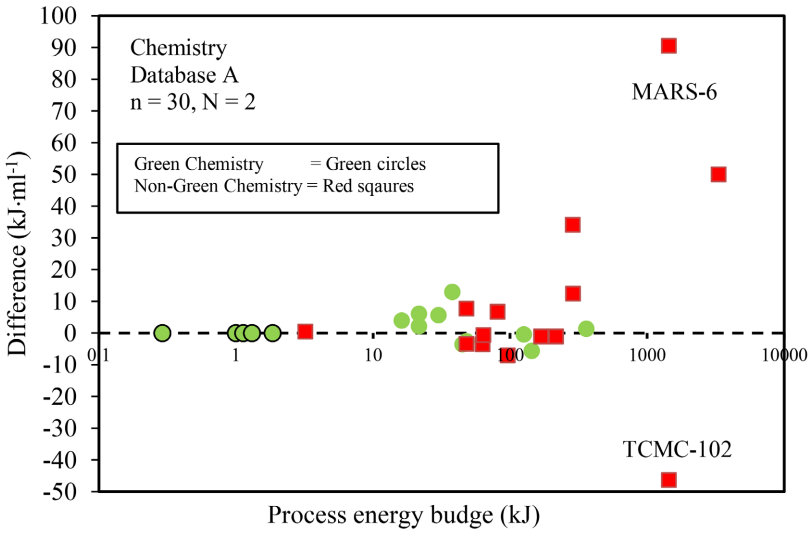

Figure 6. Database A; residual error analysis for and claimed Green Chemistry (green circles) and Non-Green Chemistry (red squares). The non-thermal microwave-assisted dielectric heating of water (green circles with black boulder) is shown to be part of claimed Green Chemistry group.

Table 1. **Database A** (n = 30) residual error sigma test (kJ·ml^{-1}).

Applicator	±Sigma	±2 Sigma	±3 Sigma
	21.770	43.540	65.310
Data points	26	3	1
Percentage	86.68%	9.99%	3.33%

power, and process time given in the incorporated eighteen publications within **Database B**. No attempt is given here to quality the quality of the nanostructure product outcome.

4.1. Palladium Dataset

Elazab *et al.* (2014) [39] used a unspecified microwave oven (rated at 1000 W) for the synthesis Pd nanoparticles supported on metal oxide (Fe_3O_4, Co_3O_4, and $Ni(OH)_2$) nanoplates. Palladium nitrate was used as the Pd precursor and $Fe(NO_3)_3{\cdot}9H_2O$, $Ni(NO_3)_2{\cdot}6H_2O$, $Co(NO_3)_2{\cdot}6H_2O$, as the metal oxides. To each suspension 600 µl of reducing agent (hydrazine hydrate) and 20 ml of deionized H_2O water added. These suspensions were then irradiated in 60 second cycles for a total process time of: 7 min ($PdFeO_x$), 5 minutes ($PdCoO_x$), and 9 minutes ($PdNiO_x$). In 2018, Elazab and Sadek (2018) [40] also used a domestic microwave oven to synthesis Pd nanoparticles supported on copper oxide (CuO). Rademacher *et al.* (2020 [41] used a CEM Discover2 applicator for synthesis of Pd nanoparticles supported on a 2,6-dicyanopyridine-covalent triazine framework (DCP-CTF). The reactants consisted of 94 µml of Pt acetylacetonate, Pd $(acac)_2$, 20 mg of DCP-CTF and 2 g of 1-butyl-3-methylimidazolium bis(trifluoromethylsulfonyl)imide. This mixture was then microwave irradiated for 20 minutes at 100 W (250˚C). See Section 4 for process energy budget comparison with Au nano-rod synthesis in the Discover2 applicator operating in the continuous flow mode [8] and [42].

4.2. Platinum Dataset

Li and Komarneni *et al.* (2006) [43] reported the use of MARS-5 (rated at 1200 W) for the synthesis of Pt nanoparticles and nano-rods. Dihydrogen hexachloroplatinate (IV) was used as the metal precursor, dissolved in 9 ml of methanol and 1 ml distilled H_2O, to which the reducing agent polyvinylpyrrolidone (PVP) was added. The MARS-5 software was used to ramp-up and hold the microwave power to achieve the following synthesis conditions irradiation of 60 minutes at 190˚C and 200 psi (13.75 bar). With the unavailability of the actual power supplied to the reactants, a value of 900 W (75% of 1200 W) is used to estimate the process energy budget [8]. Kundu *et al.* (2011) [44] used an unspecified domestic microwave oven to synthesis Pt-graphene hybrid nanostructures. The reactants used were 5 mg of grapheme oxide dissolved in 20 ml of ethylene glycol ($C_2H_4(OH)_2$) followed by the addition of 2 mg of Platinum chloride ($H_2PtCl_6{\cdot}3H_2O$). The suspension was the microwave irradiated at 800 W heating for four cycles of 50 second on-period and 10 seconds off-period which equate to irradiation time of 200 seconds. Wojnicki *et al.* (2021) [45] used the ERTEC (rated at 600 W) to synthesis Pt nanoparticles. A process suspension of 20 ml made up from the platinum precursor H_2PtCl_6 salt dissolved in H_2O and the reducing agent tri-sodium citrate salt dissolved in deionized H_2O. The synthesis conditions used was 600 W cavity-magnetron power that was pulse width modulated into three periods (360, 60 and 60 seconds) to give a total process time of approximately

500 seconds at maximum 225˚C and maximum modulated pressure between 45 and 50 bar. Pal *et al.* (2014) [20] used a Samsung CE2877 (rated at 850 W) domestic microwave oven to synthesis Pt nanoparticles. The reactants used where: Aqueous $H_2PtCl_6{\cdot}3H_2O$ mixed with 2 ml of glucose ($C_6H_{12}O_6$), and 0.1 ml of PVP, all mixed in a 50 ml Pyrex flask. The suspension was irradiated at 53% duty cycle, or 450 W for a total of 180 seconds using 30 second irradiation installments to prevent of pressure within the flask. For comparison Pal *et al.* (2014) [21] used the same microwave oven for synthesis of Ag nanoparticles (see **Figure 8**, and associated text). In this case, 10 ml of $AgNO_3$ and 1 ml of Benszo-18-crown-6 reducing and stable agent were irradiated at 35% duty cycle, or 300 W for a total of 180 seconds using 30 second irradiation installments.

4.3. ZnO Dataset

Cao *et al.* (2004) [46] used a LG-MS207T (rated at 700 W) domestic microwave oven for the synthesis of flower-like ZnO nonosheets. The syntheses used a preset 30% duty cycle (210 W) for a process time of 10 minutes with a stated duty cycle of "*on for 5 mins, off for 30* s". Li *et al.* (2011) [47] used a domestic microwave oven (type unspecified, but rated at 500 W) combined with discontinues ultrasonic treatment for a process time of 30 minutes to synthesis Zn nano-flower structures. The stating materials used where zinc acetate hydrate ($Zn(CH_3COO)_2{\cdot}2H_2O$) dissolved in 40 ml sodium hydroxide (NaH) aqueous solution. A scanning electron microscope (SEM) was used to conform and characterize the nano-flower structures. Cao *et al.* (2011) [48] used a Galanz (rated at 850 W) domestic microwave oven to synthesis nano-flowers structures. The synthesis used 6 g of zinc nitrate ($Zn(NO_3)_2{\cdot}6H_2O$)) dissolved in 2 ml of distilled H_2O, and urea ($C_2H_5NO_2$) at three different molar ratios (1:1, 5:1, and 3:1). A number of these suspensions where further mixed in zinc nitrate stock solution to form a paste. Optimal synthesis conditions (minimal aggregation) were estimated occur at a preset 40% duty cycle (340 W) for a few minutes when a urea/Zn^{2+} molar ratio of 1:1 was used. Using these reported conditions it is reasonable to assume that approximately 10 ml of suspension was used with irradiated time of 10 minutes. Li *et al.* (2014) [49] used a TCMC system (MAS-II, shanghai Xinyi Ltd) containing a mixture of $Zn(NO_3)_2{\cdot}6H_2O$ and hexamethylenetetramine ($(CH_2)_6N_4$) dissolved in 50 ml of distilled H_2O plus 2 ml of aqueous ammonia ($NH_3{\cdot}H_2O$). This suspension was then microwave irradiated at 300 W for a process time of 10 minutes. By 2015, Hasanpoor *et al.* [50] used a LG-MS1040SM (rated at 850 W) domestic microwave oven to synthesis ZnO nano-flowers structures with a controlled morphology. The microwave synthesis used a suspension of Zn nitrate hydrate ($Zn(NO_3)_2{\cdot}6H_2O$) and $NH_3{\cdot}H_2O$ dissolved in 100 ml of H_2O. Two separates suspensions (labeled: A1 and A2) were microwave irradiated at 510 and 680 W for a fixed process time of 15 and 10 minutes, respectively. After washing and drying their reaction products, SEM imaging revealed that the lower power setting (sample A1) produced nano-rods,

while the higher power setting (sample A2) produces nano-flower structures. In 2016, Krishnapriya *et al.* [51] used an Anton Paar microwave Pro applicator (rated at 900 W) that contained 8 to 48 reactions vessels on the turntable). The starting material comprised a 1:1 volume ratio of $Zn(CH_3COO)_2{\cdot}2H_2O$ and ammonium hydroxide dissolved in an unspecified amount of doubled distilled H_2O to synthesis ZnO jasmine-flower-like structures. A fixed microwave irradiation mode of 300 W (software controlled 2 minute ramp-up time and a 2 minutes hold time for a target temperature of 70˚C was found to provide optimum synthesis conditions. Using the knowledge of the Anon Paar Multiwave applicator [17] [51], a 6 ml aliquot is used to estimate the process energy density. In 2018, Wojnarowicz *et al.* [52] reported on the microwave-assisted cobalt (Co) doping of ZnO nanostructures ($Zn_{1-x}Co_xO$) using the ERTEC microwave applicator. The metal precursors used were: $Zn(CH_3COO)_2{\cdot}2H_2O$ and cobalt acetate ($Co(CH_3COO)_2{\cdot}4H_2O$) powders dissolved in 450 ml of $C_2H_4(OH)_2$, that was then dived into 75 ml aliquots for synthesis. The synthesis conditions used a preset 100% duty cycle (600 W) for a process time of 25 minutes at 190˚C and approximately 4 bar operating pressure [53]. Liu *et al.* (2019) [54] synthesized Ag decorated Zn nano-flower composite using an unspecified domestic microwave oven. The reactants comprised $Zn(CH_3COO)_2{\cdot}2H_2O$ and sodium peroxide (Na_2O_2) dissolved in 50 ml of distilled H_2O. During the microwave irradiation an unspecified amount of $AgNO_3$ in $C_2H_4(OH)_2$ was added. The microwave synthesis was carried at 400 W for 5 minutes. Aljaafari *et al.* (2020) [55] used an un-specified Samsung (rated at 750 W) domestic microwave oven containing $Zn(CH_3COO)_2{\cdot}2H_2O$ and potassium hydroxide (KOH) dissolved in 100 ml of distilled H_2O for the synthesis of ZnO flower-like nano-rod structures. The synthesis used a preset 25% duty cycle (180 W) for a process time of 20 minutes. Lastly, Cai and Hung (2023) [56] synthesized flower-like ZnO structures in a domestic microwave oven (Galanz P7ODIOP-TE, cavity-magnetron rated CW power not given). The reaction products were: $ZnCl_2$ dissolved in 200 ml of H_2O plus 30 ml of $NH_3{\cdot}H_2O$, and the ammonia water was added. Using a preset 340 W and bracketed irradiation time experiments, it was observed that ZnO flower-like structure product approached completion after 10 minutes of irradiation.

Following on from the **Database A** residual error analysis, the residual error analysis within **Database B** is explored for; applicator-type **Figure 7**; water-MO and metal precursor **Figure 8**; and claimed Green Chemistry and non-Green Chemistry **Figure 9**. Here it is impotent to the residual error values have changed due to the new 0-B model identity-line.

Figure 7 shows the applicator-type analysis using six colored coded groups (water MO, NS-discover 2, NS-MO, NS-TCMT, NS-ERTEC, and NS-Digestion), and where MO refers to microwave oven and NS refers to nanostructures. Visually it is observed that the data points follow the non-null distribution around the model identity-line. As there are no additional water-MO (open circles) data points the distribution closely resembles **Database A**. The NS-Discover2 group

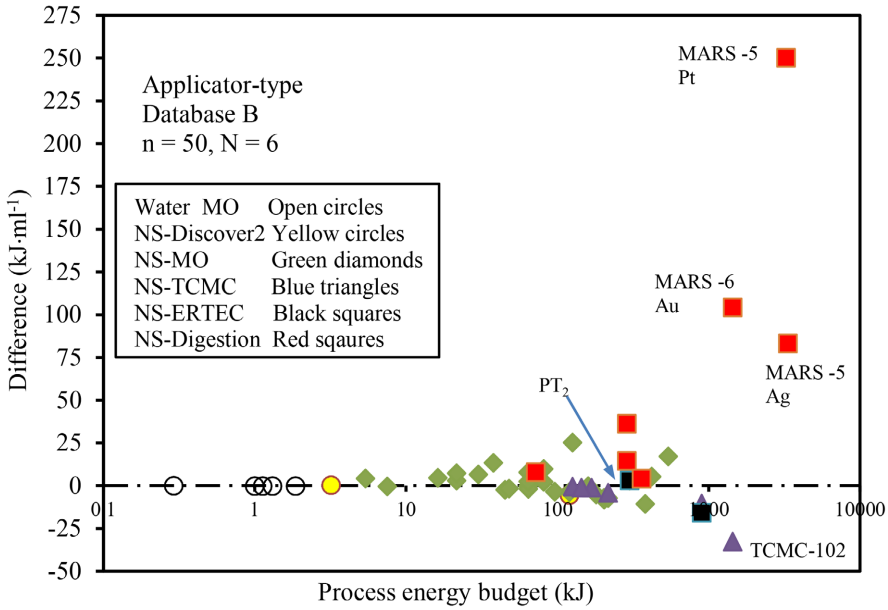

Figure 7. Database B; residual error analysis for applicator-type (water-MO, NS-Discover2, NS-MO, NS-TCMT, NS-ERTEC, and NS-Digestion. The abbreviations: MO, NS, and PT_2 refer to microwave oven, nanostructures, and possible second phase transition, respectively.

(yellow circles) has one new data point positioned at 120 kJ, −5351 kJ·ml^{-1} that is operating in the batch mode rather than the continuous mode [42]. The NS-MO group (green diamonds) has been enlarged by thirteen resulting in an enlargement of cluster around the identity-line. The NS-TCMC group (blue triangles) has also been enlarged by one and ranges in positioned at 900 kJ, +0.3 to −15 kJ·ml^{-1}. Of note, is the TCMC-102 applicator [47] that has the largest process energy budget (1440 kJ) and the most negative residual error (−32.5 kJ·ml^{-1}). The new NS-ERTEC applicator [45] [52] group is positioned in the region of 300 to 900 kJ, −10.381 kJ·ml^{-1}. Lastly the NS-Digestion applicator group (red squares) has been increased by two [43] [51] to maintain an open cluster with an MARS-5 digestion applicator [43] providing the greatest positive disagreement (+245.5 kJ·ml^{-1}).

Although the microwave applicator-type residual error plot as presented in **Figure 7** is a valid representation of the difference from the model identity-line, an alternative mapping operation is to rank the applicator-type difference by magnitude and sign to their numerical value within the database [13]. In general the main advantage of this representation is that outliers are always delineated at the two extremes and therefore easily identified. However the main disadvantage of this representation is that PTs are smothered out due to the sequential ranking operation. **Figure 8** shows this mapping operation using the same color coding as in **Figure 7**. Using this representation the 50 data point form a slow sign curve along the model identity-line, with the negative magnitudes to the left hand side and the positive magnitudes to the right hand side. The notable feature of note are that the NS-TCMC applicator group is spread out to the left, the

NS-Digestion applicator group is spread to the right and the water-MO applicator group positioned in the middle. The two data points of the NS-ERTEC group are spread away from each other.

Turning to the NS-MO group, this group is not contaminated, positioned in the middle of the ranked data and close to model identity-line. Again with water being a universal polar solvent, and considered as nontoxic and environmentally, it is included in the Green Chemistry group. With this unique position, the water-MO group can used a reference point within the dataset.

Figure 9 shows the water-MO and metal NS precursor analysis using six

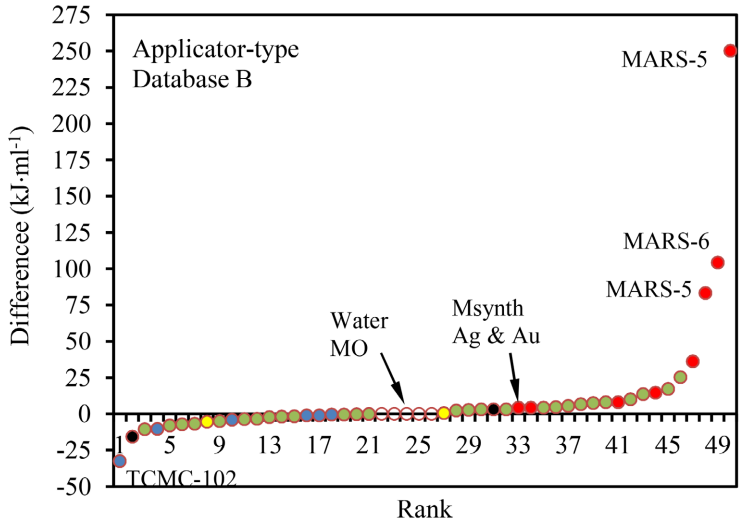

Figure 8. Database B; applicator-type ranked according to their difference from the model identity-line. water-MO (open circles), NS-Discover2 (yellow circles), NS-MO (green circles), NS-TCMT (blue circles), NS-ERTEC (black circles, and NS-Digestion (red circles).

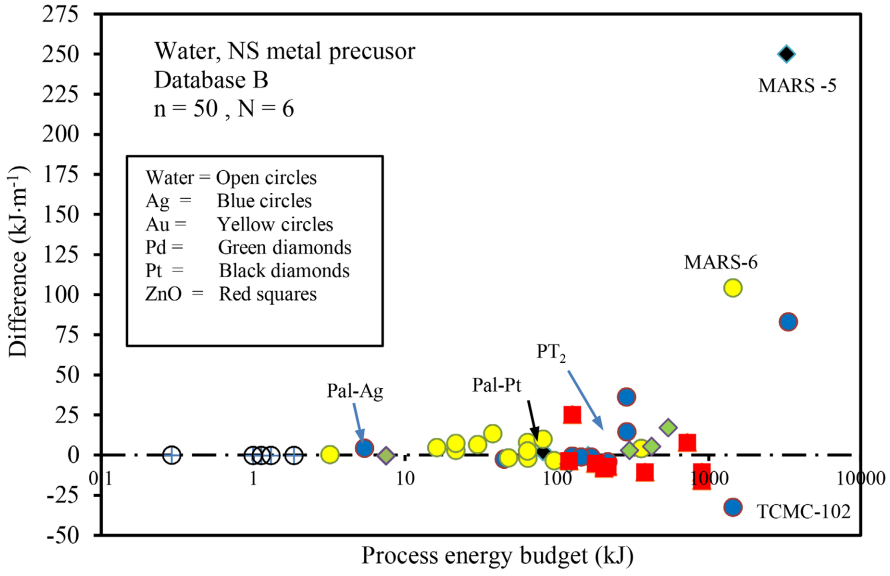

Figure 9. Database B; residual error analysis for water and NP metals. The abbreviations: PT_2 refer to possible second phase transitions; Pal-Pt and Pal-AG refers the Samsung CE2877 microwave oven synthesis of Pt and Ag, respectively.

colored coded groups (water, Au, Ag, Pd, Pt, and ZnO). The MO and NS notation has the same meaning as before. Visually the data has the same non-null distribution as Figure 7, but with a change in individual color according to their new grouping. Again the non-thermal microwave-assisted dielectric heating of water group (open circles) has no additional data, therefore acts as reference group. The Ag precursor group (blue circles) are now revealed to range from a microwave oven applicator (5.4 kJ, +2 kJ·ml^{-1}) to the TCMC-102 (1440 kJ, −33.3 kJ·ml^{-1}), and on to a MARS-5 digestion applicator (3330 kJ, +78.3 kJ·ml^{-1}). The Au precursor group (yellow circles) ranges from the Discover2 applicator (3.2 kJ, +0.527 kJ·ml^{-1}) to the MARS-6 applicator (1440 kJ, +103.4 kJ·ml^{-1}). The Pd precursors (green diamond) range between a microwave oven applicator (7.5 kJ, −0.215 kJ·ml^{-1}), to a microwave oven (540 kJ, +17.3 kJ·ml^{-1}). The Pt precursors (black diamond) range from a microwave oven (81 kJ, +2.8 kJ·ml^{-1}) to an ERTEC applicator (300 kJ, +3.3 kJ·ml^{-1}). Finally, the ZnO precursors (red squares) range from a microwave oven (120 kJ, −3.5 kJ·ml^{-1}) to an ERTEC applicator (900 kJ, −33.3 kJ·ml^{-1}).

Now consider the comparison of the Samsung CE2877 microwave oven claimed Green Chemistry synthesis of Pt [20] and non-Green Chemistry synthesis of Ag [21] nanostructures. These metals are annotated as Pal-Pt (black diamond) and (Pal-Ag (blue circle) in Figure 8. In terms of process energy budget Pt uses 81 kJ, as compared to 5.4 kJ for Ag, however the residual error are close to 2 kJ·ml^{-1} of the model identity-line, therefore having similar energy transfer efficiencies.

Further consider the two Discover2 applicators, one operating in the continuous flow mode [42] and one operating in batch mode [41]. The continuous flow mode applicator is efficient according to the 0-D model with +0.5 kJ·ml^{-1}, whilst the batch mode applicator is less efficient −4.9 kJ·ml^{-1}. Here the efficiency is due to the low applied power (36 W) and short residence time of 1.5 minutes used in the continuous flow mode.

Figure 10 shows the claimed Green Chemistry (green circles) and non-Green Chemistry (red squares). Again, the universal polar solvent and nontoxic and environmentally benign properties of water, allows the non-thermal microwave-assisted dielectric heating of water data is included in the claimed Green Chemistry group. Visually the data has the same non-null distribution as Figure 7 and Figure 8, but with a change in individual color code according to their new grouping. Given this adjustment the claimed Green Chemistry group process energy budget ranges from 0.291 to 900 kJ, with a residual error ranging between −33 to +25.9 kJ·ml^{-1}. The non-Green Chemistry group however has a higher process energy budget. For example: The MARS-5 that uses polyvinylpyrrolidone (PVP) with the either methanol or ethanol has process energy value some 3.2 MJ, the MARS-6 that uses $NaBH_4$ has a process energy budget of 3.3 MJ, and the MARS-5 that uses Na_2SnO_3 has a process energy budget of 3.3 MJ.

A visual comparison of the residual error data in Figures 7-10 indicate that the possible presence of PT_1 diminishes with increased sample size. However,

the possible PT_2 is still observed between the NS-TCMC and the NS-Digestion group boundaries. In addition the Sigma test Table 2 reveals that the power-law residual error still has a uniform distribution (non-bell shaped) with forty seven (94%) data points within ± sigma, two (4%) within the ± 2 to ± 3 Sigma and one (2%) at the ± 3 Sigma limit. Moreover the problematic MARS-5 applicator data becomes located between +2 and +3 sigma limits therefore losing its problematic outlier candidacy. This candidacy is now taken over by the new MARS-6 applicator [18].

5. 2-D Cluster Analysis of Applicator Group

Euclidean and Manhattan distance function are two of the commonly used metric to define a cluster of data points and identify problematic outlier [57] [58] and [59]. In this section a simple method of cluster analysis is proposed that uses the Excel spread sheet format (row and columns) populated by data points, and where formula functions (=SUM (MAX, MIN, AVERAGE, and STDEV)) are used to calculate the following three cluster metrics;

1) Energy area (kJ × kJ·ml^{-1} = kJ^2·ml^{-1})

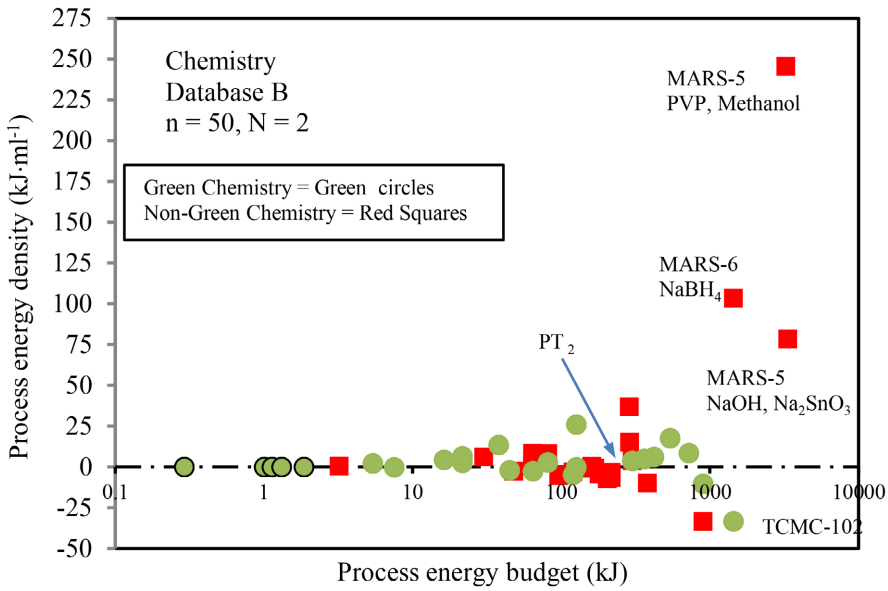

Figure 10. **Database B**; residual error analysis of water-MO, claimed Green Chemistry, and non-Green Chemistry. The non-thermal microwave-assisted dielectric heating of water data (green circles with black outline) is shown to be part of claimed Green Chemistry group.

Table 2. **Database B** (n = 50) residual error sigma test (kJ·ml^{-1}).

Applicator	±Sigma	±2 Sigma	±3 Sigma
	40.487	80.961	121.441
Data points	47	2	1
Percentage	94%	4%	2%

2) Group (N) density (energy area divided by the number data points, n)

3) Group (N) x, y arithmetic mean

As PT_1 has been shown to diminish with sample size, only **Database B** is explored for problematic outliers using the three cluster metrics. Figure 11 shows the results of three cluster metrics as applied to the **Database B** residual error plot. The six semi-transparent (60%) color areas (clear, yellow, green, blue black and red are the applicator type) represent the respective applicator-type group energy areas and the bold plus signs denote the arithmetic mean of each group area. Also shown is the +3 sigma line and region of possible PT_2. The metrics numeric values are given are given in Table 3.

The first feature of note within Figure 11, as with Figure 7, Figure 8, and Figure 10, is the water-MO group separated from the other 5 applicator-type groups along the model identity-line. The second feature of note is that the data point falls within ± sigma. Now consider the new NS-ERTEC applicator area and arithmetic mean data, both of which contaminate the NS-TCMC applicator group and the NS-Digestion application group in the 300 to 900 kJ range. This mixing of datasets and the possible PT_2 location where the NS-Digestion applicator group exhibits a marked increase in residual error suggest two scenarios. First the underlying energy transfers mechanism (first-order to second-order reaction kinetics) is changing between applicator-types, or, poor reporting of the real Digestion applicator energy profile that is due to a lack of knowledge of how the preparatory software controls the Digestion applicator cavity-magnetron.

Now consider the NS-Digestion applicator-type group that contains the

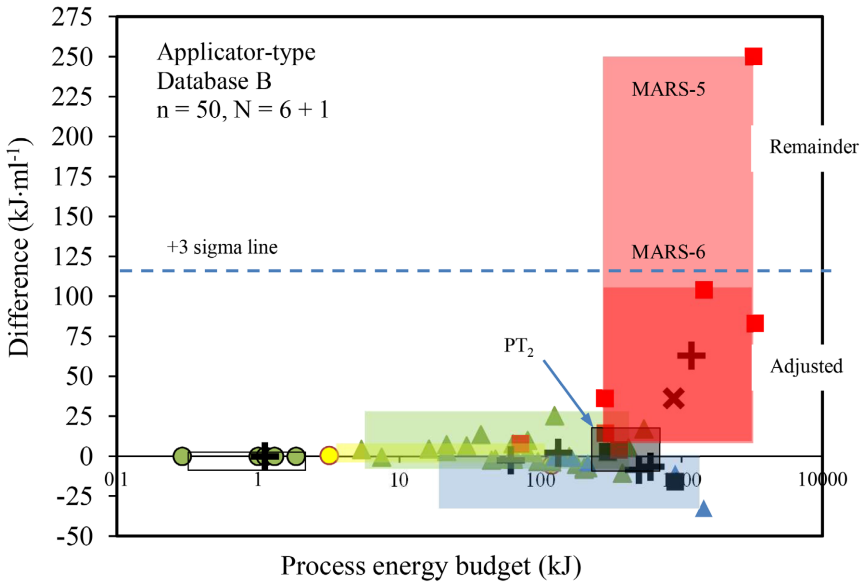

Figure 11. Database B; residual error parametric cluster analysis of the original six applicator groups. water-MO (green circles with black outline), NS-Discover2 (yellow circle), NS-MO (green triangles), NS-TCMC (blue triangles), and NS-Digestion (red squares). The bold plus signs represent their mean x, y coordinate. The bold cross sign represents mean x, y coordinate of adjusted NS-Digestion group within the darker red represents the adjusted energy area.

problematic MARS-5 applicator. Before adjustment the group has a area density of 101,485.5 $kJ^2 \cdot ml^{-1}$ per data point, when the group is adjusted by removing the problematic MARS-5 applicator data point, the area deceases by factor 2.15 to 47,178.9 $kJ^2 \cdot ml^{-1}$ per data point. The corresponding arithmetic mean also moves from x = 1172.1 kJ, y = +66.1 $kJ \cdot ml^{-1}$ to x = 876.1 kJ, y = +36.4 $kJ \cdot ml^{-1}$. In this cleaning/filtering process, the filtered MARS-5 applicator now has a notional area density of 481,636.6 $kJ^2 \cdot ml^{-1}$ per data point, an increase in area of ten times per data point.

6. Allometric Scaling

Assuming that the microwave-assisted synthesis power-laws are Scale Free, an estimation of allometric scaling is now performed Table 4. In this table, the average of the three databases are computed and yield an allomteric scaling of 0.7172 ± 0.3214 $kJ \cdot ml^{-1}$ at x = 0.001 kJ, and exponent = 0.791 ± 0.055, or approximately 3/4. This computed average value for the exponent has a hypoallometric trait that falls within close to the bibliometric scaling laws for scientific fields (0.87 to 1.01 [13] and within reported physiological (relative body mass)

Table 3. **Database B**; parametric cluster analysis of applicator-type groups.

Applicator group	Number of data points (n)	Energy area ($kJ^2 \cdot ml^{-1}$)	Cluster density ($kJ^2 \cdot ml^{-1}$/n)	Mean x coordinate (kJ)	Mean y coordinate ($kJ^2 \cdot ml^{-1}$)
Water-MO	**5**	0.0467	0.009	1.1	−51.6
Discover2	**2**	169.0	84.5	61.6	−2.4
NS-MO	**27**	19,181.7	710.4	133.2	2.3
NS-TCMC	**6**	50,194.8	8365.8	499.0	−8.3
NS-ERTEC	**2**	24,649.9	12,324.9	600.0	−6.3
NS-Digestion	**8**	811,884.2	101,485.5	1172.1	63.1
		Adjusted NS-Digestion group			
NS-Digestion	**7**	330,250.1	47,178.9	876.1	36.4
		Cleaned or filter applicator			
NS-Digestion	**1**	14.9	481,636.6	3240.0	250.1

Table 4. Estimated allometric scaling of microwave-assisted synthesis of Pd, Ag, Pt, Au, and ZnO nanostructures.

Database	Power-law
Database A (n = 30)	$y = 0.3293x^{0.846}$
Database B (n = 50)	$y = 0.7837x^{0.764}$
Database B$_{adjusted}$ (n = 49)	$y = 1.0386x^{0.764}$
Average of the three databases	$y = 0.7172 \pm 0.3214x^{0.791 \pm 0.055}$

scaling laws (0.7 to 0.92 [10] [11]).

7. Summary and Outlook

This paper is the second in the series of microwave-assisted synthesis power-law signature studies over 4 order of magnitude relating to process energy budget (kJ) relationship and energy density (kJ·ml^{-1}). Two historical databases are investigated, **Database A** (n = 30) relating Au and Ag nanostructure synthesis [8], **Database B** (n = 50) containing n = 20 new datasets relating Pd, Pt and ZnO nanostructures. Microsoft Excel Linear regression analysis is applied to **Database A** and **B** to generate power-law 0-D model ($y = cx^n$) to provide a horizontal 0-D model identity-line from which the residual error (measured in ± kJ·ml^{-1}) is obtained. The residual error is explored in null and rank plot format as a function six microwave applicator–types (domestic microwave oven, TCMC oven, Digester, axial field helical antenna (disover2, and ERTEC). In addition residual error analysis is performed on the five metal precursors, along with their claimed Green Chemistry and non-Green Chemistry.

The findings of this study are summed as follows:

1) The original Au and Ag database (n = 30) [8] and new database containing Pd, Pt and ZnO (n = 50) and (adjusted Database (n = 49) yield a global microwave-assisted synthesis 0-D model over four order of magnitude with constants of c = 0.7172 ± 0.3214 kJ·ml^{-1} at x-axes = 0.001 kJ, with an exponent = 0.791 ± 0.055, approximately 3/4.

2) It is noted the constant c within the 0-D model is a mathematical construct that does not exist in reality due to the warm-up time of the cavity-magnetron (approximately 3 seconds [7]). Thus for a cavity-magnetron rated at 800 W operating in CW mode, the estimated process energy budget lower limit (x_{min}) equates to 800 multiplied by 3 = 2.4 kJ. This is an important observation when allometric scaling principles are employed as c has generally been ill defined [10] [11] [12] and [13].

3) Phase-transitions are observed to be reduced with sample number (30 to 50) to leave one permanent PT_2 that is aligned to excess positive process energy density residual error valves associated with the Digestion applicator-type group. This group of applicator have inbuilt software to control temperature and pressure targets. But their operation has lead to poor reporting of the applied power and energy profile over process time, from which it is thought an error in the initial energy calculation, carries though to the observed residual error. The high positive residual error values associated with the loaded turntable and its sealed reaction vessels where cumulated heat produces a second-order effect.

4) Statistical analysis and cluster analysis is used to detect outliers. This knowledge is used with a detailed understanding of the outlier origins, to direct cleaning/filtering of the problematic outliers from the database.

5) A comparison of Claimed Green Chemistry and non-Green Chemistry has been performed, and found that Claimed Green Chemistry process (which here

includes the non-thermal microwave-assisted dielectric heating of water) have a generally greatly reduced process energy budgets. The non-Green Chemistry synthesis has a higher process energy budget ranging from 3.2 kJ to 3.3 MJ.

The statistical analyses and parametric cluster analyses performed on the historical microwave-assisted database provides a new outlook in the field of microwave-assisted synthesis of transition metal-nanostructures. This work gives researchers a wider and better understanding of the energy process involved, all of which are hidden within the historical published microwave-assisted synthesis records. The use of a power-law signature calibration allows researchers to scale-out working microwave-assisted processes with focus on process intensification; *i.e.*, choosing a microwave applicator with one cavity-magnetron rather than two cavity-magnetrons, or by reducing the applicator size; thereby reducing energy use and increasing energy efficiency. The power-law signature also allows new synthesis to be developed with the six principle of Green Chemistry embedded at the start of the design process. In addition, with focus on the understanding and reporting of the process energy profile (not just temperature and pressure targets) when using software controlled microwave applicators. Finally in relation to process intensification, only one of the 50 microwave applicators mentioned in this study is operated in the continuous mode. Clearly more attention to continuous flow mode syntheses is required.

Acknowledgements

We would like to thank the delegates of the 16th Chaos 2023 International Conference 13th to 16th June 2023 (Hellenic Mediterranean University. Heraklion, Crete, Greece) for their discussions and support in the preparation of this work.

Conflicts of Interest

The authors declare no conflicts of interest regarding the publication of this paper.

References

[1] Gedye, R.N., Smith, F. and Westaway, K.C. (1988) The Rapid Synthesis of Organic Compounds in Microwave Ovens. *Canadian Journal Chemistry*, **66**, 17-26. https://doi.org/10.1139/v88-003

[2] Gedye, R.N., Rank, W. and Westaway, K.C. (1991) The Rapid Synthesis of Organic Compounds in Microwave Ovens. II. *Canadian Journal Chemistry*, **69**, 706-711. https://doi.org/10.1139/v91-106

[3] Rinaldi, L., Carnaroglio, D., Rotolo, L. and Cravotto, G. (2015) A Microwave-Based Chemical Factory in the Lab: From Milligram to Multigram Preparations. *Journal of Chemistry*, **2015**, Article ID: 879531. https://doi.org/10.1155/2015/879531

[4] Grewal, A.S., Kumar, K., Redhu, S. and Bhardwaj, S. (2013) Microwave Assisted Synthesis: A Green Synthesis Chemistry Approach. *International Research Journal of Pharmaceutical and Applied Sciences*, **3**, 278-285.

[5] Priecel, P. and Lopez-Sanchez, J.A. (2018) Advantages and Limitations of Micro-

wave Reactors: From Chemical Synthesis to the Catalytic Valorization of Biobased Chemicals. *ACS Sustainable Chemistry and Engineering*, **7**, 3-21. https://doi.org/10.1021/acssuschemeng.8b03286

[6] Law, V.J. and Dowling, D.P. (2022) Microwave-Assisted Inactivation of Fomite-Microorganism Systems: Energy Phase-Space Projection. *American Journal Analytical Chemistry*, **13**, 255-276. https://doi.org/10.4236/ajac.2022.137018

[7] Law, V.J. and Dowling, D.P. (2023) Revisiting "Non-Thermal" Batch Microwave oven Inactivation of Microorganisms. *American Journal of Analytical Chemistry*, **14**, 28-54. https://doi.org/10.4236/ajac.2023.141003

[8] Law, V.J. and Dowling, D.P. (2023) Microwave-Assisted Au and Ag Nanoparticle Synthesis: An Energy Phase-Space Projection Analysis. *American Journal Analytical Chemistry*, **14**, 149-174. https://doi.org/10.4236/ajac.2023.144009

[9] Hanel, R., Corominas-Murtra, B., Liu, B. and Thurner, S. (2017) Fitting Power-Laws in Empirical Data with Estimators That Work for All Exponents. *PLOS ONE*, **12**, e0170920. https://doi.org/10.1371/journal.pone.0170920

[10] Huxley, J.S. and Teissier, G. (1936) Terminology of Relative Growth. *Nature*, **137**, 780-781. https://doi.org/10.1038/137780b0

[11] Calder III, W.A. (1981) Scaling of Physiological Processes in Homeothermic Animals. *Annual Review of Physiology*, **43**, 301-322. https://doi.org/10.1146/annurev.ph.43.030181.001505

[12] Stumpf, M.P.H. and Porter, M.A. (2012) Critical Truths about Power Laws. *Science*, **355**, 665-666. https://doi.org/10.1126/science.1216142

[13] Dong, H., Li, M., Liu, R., Wu, C. and Wu, J. (2017) Allometric Scaling in Scientific Fields. *Scientometrics*, **112**, 583-594. https://doi.org/10.1007/s11192-017-2333-y

[14] Blosi, M., Albonetti, S., Gatti, F., Dondi, M., Migliori, A., Ortolani, L., Morandi, V. and Baldi, G. (2010) Au, Ag and Au-Ag Nanoparticles: Microwave-Assisted Synthesis in Water and Applications in Ceramic and Catalysis. *Nanotech*, **1**, 352-355.

[15] Rai, P., Majhi, S.M., Yu, Y.T. and Lee, J.H. (2015) Synthesis of Plasmonic Ag@SnO_2 Core-Shell Nanoreactors for Xylene Detection. *RSC Advances*, **5**, 17653-17659. https://doi.org/10.1039/C4RA13971B

[16] Alfano, B., Polichetti, T., Mauriello, M., Miglietta, M.L., Ricciardella, F., Massera, E. and Francia, G.D. (2016) Modulating the Sensing Properties of Graphene through an Eco-Friendly Metal-Decoration Process. *Sensors and Actuators B: Chemical*, **222**, 1032-1042. https://doi.org/10.1016/j.snb.2015.09.008

[17] Miglietta, M.L., Alfano, B., Polichetti, T., Massera, E., Schiattarella, C. and Di Francia, G. (2018) Effective Tuning of Silver Decorated Graphene Sensing Properties by Adjusting the Ag NPs Coverage Density. In: Andò, B., Baldini, F., Di Natale, C., Marrazza, G. and Siciliano, P., Eds., *CNS* 2016: *Sensors*, Springer, Cham, 82-89.

[18] Marinoiu, A., Andrei, R., Vagner, I., Niculescu, V., Bucra, F., Constantinescu, M. and Carcadea, E. (2020) One Step Synthesis of Au Nanoparticles Supported on Graphene Oxide Using an Eco-Friendly Microwave-Assisted Process. *Materials Science*, **26**, 249-254. https://doi.org/10.5755/j01.ms.26.3.21857

[19] Gonçalves, R.A., Toled, R.P., Joshi, N. and Berengue, O.M. (2021) Green Synthesis and Applications of ZnO andTiO_2 Nanostructures. *Molecules*, **26**, Article 2236. https://doi.org/10.3390/molecules26082236

[20] Pal, J., Deb, M.K., Deshmukh, D.K. and Sen, B.K. (2014) Microwave-Assisted Synthesis of Platinum Nanoparticles and Their Catalytic Degradation of Methyl Violet in Aqueous Solution. *Applied Nanoscience*, **4**, 61-65.

https://doi.org/10.1007/s13204-012-0170-0

[21] Pal, J., Deb, M.K. and Deshmukh, D.K. (2014) Microwave-Assisted Synthesis of Silver Nanoparticles Using Benzo-18-Crown-6 as Reducing and Stabilizing Agent. *Applied Nanoscience*, **4**, 507-510. https://doi.org/10.1007/s13204-013-0229-6

[22] Harpeness, R. and Gedanken, A. (2004) Microwave Synthesis of Core-Shell Gold/Palladium Bimetallic Nanoparticles. *Langmuir*, **20**, 3431-3434. https://doi.org/10.1021/la035978z

[23] Abdelsayed, V., Aljarash, A. and El-Shall, M.S. (2009) Microwave Synthesis of Bimetallic Nanoalloys and Co Oxidation on Ceria-Supported Nanoalloys. *Chemistry of Materials*, **21**, 2825-2834. https://doi.org/10.1021/cm9004486

[24] Siamaki, A.R., Khder, A.E.R.S., Abdelsayed, V., El-Shall, M.S. and Gupton, B.F. (2011) Microwave-Assisted Synthesis of Palladium Nanoparticles Supported on Graphene: A Highly Active and Recyclable Catalyst for Carbon-Carbon Cross-Coupling Reactions. *Journal of Catalysis*, **279**, 1-11. https://doi.org/10.1016/j.jcat.2010.12.003

[25] Rai, P., Kim, S.G. and Yu, Y.T. (2012) Microwave Assisted Synthesis of Flower-Like ZnO and Effect of Annealing Atmosphere on Its Photoluminescence Property. *Journal of Mater Science*: *Mater Electron*, **23**, 344-348. https://doi.org/10.1007/s10854-011-0384-z

[26] Prakash, T., Jayaprakash, R., Neri, G. and Kumar, S. (2013) Synthesis of ZnO Nanostructures by Microwave Irradiation Using Albumen as a Template. *Journal of Nanoparticles*, **2013**, Article ID: 274894. https://doi.org/10.1155/2013/274894

[27] Zhang, J. and Bai, X. (2017) Microwave-Assisted Synthesis of Pd Nanoparticles and Catalysis Application for Suzuki Coupling Reactions. *The Open Materials Science Journal*, **11**, 1-8. https://doi.org/10.2174/1874088X01711010001

[28] Gomez-Bolivar, J., Mikheenko, I.P., Macaskie, L.E. and Merroun, M.L. (2019) Characterization of Palladium Nanoparticles Produced by Healthy and Microwave Injured Cells of *Desulfovibrio desulfuricans* and *Escherichia coli*. *Nanomaterials*, **9**, Article 857. https://doi.org/10.3390/nano9060857

[29] Nishida, Y., Wada, Y., Chaudhari, C., Sato, K. and Nagaoka, K. (2019) Preparation of Noble-Metal Nanoparticles by Microwave-Assisted Chemical Reduction and Evaluation as Catalysts for Nitrile Hydrogenation under Ambient Conditions. *Journal of the Japan Petroleum Institute*, **62**, 220-227. https://doi.org/10.1627/jpi.62.220

[30] Yalcin, M. (2020) Microwave-Assisted Synthesis of ZnO Nanoflakes: Structural, Optical and Dielectric Characterization. *Materials Research Express*, **7**, Article ID: 055019. https://doi.org/10.1088/2053-1591/ab940f

[31] Jaimes-Paez, C.D., Vences-Alvarez, E., Salinas-Torres, D., Morallón, E., Rangel-Mendez, J.R. and Cazorla-Amorós, D. (2023) Microwave-Assisted Synthesis of Carbon-Supported Pt Nanoparticles for Their Use as Electrocatalysts in the Oxygen Reduction Reaction and Hydrogen Evolution Reaction. *Electrochimica Acta*, **464**, Article ID: 142871. https://doi.org/10.1016/j.electacta.2023.142871

[32] Andriani, P. and McKelvey, B. (2009) From Gaussian to Paretian Thinking: Causes and Implications of Power Laws in Organizations. *Perspective Organization Science*, **20**, 1053-1071. https://doi.org/10.1287/orsc.1090.0481

[33] Law, V.J., Tewordt, M., Ingram, S.G. and Jones, G.A.C. (1991) Alkane Based Plasma Etching of GaAs. *Journal of Vacuum Science & Technology B*, **9**, 1449-1455. https://doi.org/10.1116/1.585449

[34] Law, V.J., Ingram, S.G., Tewordt, M. and. Jones, G.A.C. (1991) Reactive Ion Etching

of GaAs Using CH_4: In He, Ne and Ar. *Semiconductor Science and Technology*, **6**, 411-413. https://doi.org/10.1088/0268-1242/6/5/019

[35] Kurilovich, D., *et al.* (2018) Power-Law Scaling of Plasma Pressure on Laser-ablAted Tin Microdroplets. *Physics of Plasmas*, **25**, Article ID: 012709. https://doi.org/10.1063/1.5010899

[36] Tynan, J., Law, V.J., Twomey, B., Hynes, A.M., Daniels, S., Byrne, G. and Dowling, D.P. (2009) Evaluation of Real-Time Non-Invasive Performance Analysis Tools for the Monitoring of Atmospheric Pressure Plasma. *Measurement Science and Technology*, **20**, Article ID: 115703. https://doi.org/10.1088/0957-0233/20/11/115703

[37] Law, V.J., Tynan, J., Byrne, G., Dowling, D.P. and Daniels, S. (2010) The Application of Multivariate Analysis Tools for Non-Invasive Performance Analysis of Atmospheric Pressure Plasma. In: Skiadas, C.H. and Dimotikalis, I., Eds., *Chaotic Systems: Theory and Applications*, World Scientific Publishing, Singapore, 147-154. https://doi.org/10.1142/9789814299725_0019

[38] Chen, J., Wang, J., Zhang, X. and Jin, Y. (2008) Microwave-Assisted Green Synthesis of Silver Nanoparticles by Carboxymethyl Cellulose Sodium and Silver Nitrate. *Materials Chemistry and Physics*, **108**, 421-424. https://doi.org/10.1016/j.matchemphys.2007.10.019

[39] Elazab, H.A., Moussa, S., Gupton, B.F. and El-Shall, M.S. (2014) Microwave-Assisted Synthesis of Pd Nanoparticles Supported on Fe_3O_4, Co_3O_4, and $Ni(OH)_2$ Nanoplates and Catalysis Application for CO Oxidation. *Journal of Nanoparticle Research*, **16**, Article No. 2477. https://doi.org/10.1007/s11051-014-2477-0

[40] Elazab, H.A., Sadek, M.A. and El-Idreesy, T.T. (2018) Microwave-Assisted Synthesis of Palladium Nanoparticles Supported on Copper Oxide in Aqueous Medium as an Efficient Catalyst for Suzuki Cross-Coupling Reaction. *Adsorption Science & Technology*, **36**, 1362-1365. https://doi.org/10.1177/0263617418771777

[41] Rademacher, L., Yen Beglau, T.H., Heinen, T., Barthel, J. and Janiak, C. (2020) Microwave-Assisted Synthesis of Iridium Oxide and Palladium Nanoparticles Supported on a Nitrogen-Rich Covalent Triazine Framework as Superior Electrocatalysts for the Hydrogen Evolution and Oxygen Reduction Reaction. *Frontiers of Chemistry*, **10**, Article 94526. https://doi.org/10.3389/fchem.2022.945261

[42] Bayazit, M.K., Yue, J., Cao, E., Gavriilidis, A. and Tang, J. (2016) Controllable Synthesis of Gold Nanoparticles in Aqueous Solution by Microwave Assisted Flow Chemistry. *ACS Sustainable Chemistry & Engineering*, **4**, 6435-6442. https://doi.org/10.1021/acssuschemeng.6b01149

[43] Li, D. and Komarneni, S. (2006) Synthesis of Pt Nanoparticles and Nanorods by Microwave-Assisted Solvothermal Technique. *Zeitschrift fuer Naturforschung B*, **61**, 1566-1572. https://doi.org/10.1515/znb-2006-1214

[44] Kundu, P., Nethravathi, C., Deshpande, P.A., Rajamathi, M., Madras, G. and Ravishankar, N. (2011) Ultrafast Microwave-Assisted Route to Surfactant-Free Ultrafine Pt Nanoparticles on Graphene: Synergistic Co-Reduction Mechanism and High Catalytic Activity. *Chemistry of Materials*, **23**, 2772-2778. https://doi.org/10.1021/cm200329a

[45] Wojnicki, M., Luty Błocho, M., Kwolek, P., Gajewska, M., Socha, R.P., Pędzich, Z., Csapó, E. and Hessel, V. (2021) The Influence of Dielectric Permittivity of Water on the Shape of PtNPs Synthesized in High Pressure High Temperature Microwave Reactor. *Scientific Reports*, **11**, Article No. 4851. https://doi.org/10.1038/s41598-021-84388-2

[46] Cao, J. and Wang, J. (2004) Microwave-Assisted Synthesis of Flower-Like ZnO Nanosheet Aggregates in a Room-Temperature Ionic Liquid. *Chemistry Letters*, **33**, 1332-1333. https://doi.org/10.1246/cl.2004.1332

[47] Li, H., Liu, E., Chan, F.Y.E., Lu, Z. and Chen, R. (2011) Fabrication of Ordered Flower-Like ZnO Nanostructures by a Microwave and Ultrasonic Combined Technique and Their Enhanced Photocatalytic Activity. *Materials Letters*, **65**, 3440-3443. https://doi.org/10.1016/j.matlet.2011.07.049

[48] Cao, Y., Liu, B., Huang, R., Xia, Z. and Ge, S. (2011) Flash Synthesis of Flower-Like ZnO Nanostructures by Microwave-Induced Combustion Process. *Materials Letters*, **65**, 160-163. https://doi.org/10.1016/j.matlet.2010.09.072

[49] Li, X., Wang, C., Zhou, X., Liu, J., Sun, P. and Lu, G. (2014) Gas Sensing Properties of Flower-Like ZnO Prepared by a Microwave-Assisted Technique. *Royal Society of Chemistry Advances*, **4**, 47319-47324. https://doi.org/10.1039/C4RA07425D

[50] Hasanpoor, M., Aliofkhazraei, M. and Delavari, H. (2015) Microwave-Assisted Synthesis of Zinc Oxide Nanoparticles. *Procedia Materials Science*, **11**, 320-325. https://doi.org/10.1016/j.mspro.2015.11.101

[51] Krishnapriya, R., Praneetha, S. and Murugan, A.V. (2016) Investigation of the Effect of Reaction Parameters on the Microwave-Assisted Hydrothermal Synthesis of Hierarchical Jasmine-Flower-Like ZnO Nanostructures for Dye-Sensitized Solar Cells. *New Journal of Chemistry*, **40**, 5080-5089. https://doi.org/10.1039/C6NJ00457A

[52] Wojnarowicz, J., Chudoba, T., Gierlotka, S., Sobczak, K. and Lojkowski, W. (2018) Size Control of Cobalt-Doped ZnO Nanoparticles Obtained in Microwave Solvothermal Synthesis. *Crystals*, **8**, Article 179. https://doi.org/10.3390/cryst8040179

[53] Wojnarowicz, J. (2023) Private Communication Regarding Operating Pressure of ERTEC Microwave Applicator.

[54] Liu, H., Liu, H., Yang, J., Zhai, H., Liu, X. and Jia, H. (2019) Microwave-Assisted One-Pot Synthesis of Ag Decorated Flower-Like ZnO Composites Photocatalysts for Dye Degradation and NO Removal. *Ceramics International*, **45**, 20133-20140. https://doi.org/10.1016/j.ceramint.2019.06.279

[55] Aljaafari, A., Ahmed, F., Awada, C. and Shaalan, N.M. (2020) Flower-Like ZnO Nanorods Synthesized by Microwave-Assisted One-Pot Method for Detecting Reducing Gases: Structural Properties and Sensing Reversibility. *Frontiers in Chemistry*, **8**, Article 456. https://doi.org/10.3389/fchem.2020.00456

[56] Cai, Y. and Hung, J. (2023) Preparation and Photocatalysis Characteristics of Flower-Like ZnO by Microwave Method. *Journal of Physics*: *Conference Series*, **2437**, Article ID: 012039. https://doi.org/10.1088/1742-6596/2437/1/012039

[57] Hennig, C. (2003) Clusters, Outliers, and Regression: Fixed Point Clusters. *Journal of Multivariate Analysis*, **86**, 183-212. https://doi.org/10.1016/S0047-259X(02)00020-9

[58] Loureiro, A., Torgo, L. and Soares, C. (2004) Outlier Detection Using Clustering Methods: A Data Cleaning Application. *Proceedings of KDNet Symposium on Knowledge-Based Systems for the Public Sector*, Bonn, June 2004.

[59] Lara, J.A., Lizcano, D., Rampérez, V. and Soriano, J. (2020) A Method for Outlier Detection Based on Cluster Analysis and Visual Expert Criteria. *Expert Systems*, **37**, e12473. https://doi.org/10.1111/exsy.12473